ELSEVIER

NeuroImage

www.elsevier.com/locate/ynimg
NeuroImage 30 (2006) 1100 – 1111

Characterization of displaced white matter by brain tumors using combined DTI and fMRI

Tom Schonberg,[a,b] Pazit Pianka,[b] Talma Hendler,[b] Ofer Pasternak,[c] and Yaniv Assaf[b,d,*]

[a]*Department of Psychology, Tel Aviv University, Tel Aviv, Israel*
[b]*The Levie-Edersheim-Gitter Institute for Functional Brain Imaging, Tel Aviv Sourasky Medical Center and Tel Aviv University, Tel Aviv, Israel*
[c]*School of Computer Science, Tel Aviv University, Ramat Aviv, Tel Aviv, Israel*
[d]*Department of Neurobiochemistry, Tel Aviv University, Ramat Aviv, Tel Aviv, Israel*

Received 4 August 2005; revised 6 November 2005; accepted 10 November 2005
Available online 19 January 2006

In vivo white matter tractography by diffusion tensor imaging (DTI) has become a popular tool for investigation of white matter architecture in the normal brain. Despite some unresolved issues regarding the accuracy of DTI, recent studies applied DTI for delineating white matter organization in the vicinity of brain lesions and especially brain tumors. Apart from the intrinsic limitations of DTI, the tracking of fibers in the vicinity or within lesions is further complicated due to changes in diseased tissue such as elevated water content (edema), tissue compression and degeneration. These changes deform the architecture of the white matter and in some cases prevent definite selection of the seed region of interest (ROI) from which fiber tracking begins. We show here that for displaced fiber systems, the use of anatomical approach for seed ROI selection yields insufficient results. Alternatively, we propose to select the seed points based on functional MRI activations which constrain the subjective seed ROI selection. The results are demonstrated on two major fiber systems: the pyramidal tract and the superior longitudinal fasciculus that connect critical motor and language areas, respectively. The fMRI based seed ROI selection approach enabled a more comprehensive mapping of these fiber systems. Furthermore, this procedure enabled the characterization of displaced white matter using the eigenvalue decomposition of DTI. We show that along the compressed fiber system, the diffusivity parallel to the fiber increases, while that perpendicular to the fibers decreases, leading to an overall increase in the fractional anisotropy index reflecting the compression of the fiber bundle. We conclude that definition of the functional network of a subject with deformed white matter should be done carefully. With fMRI, one can more accurately define the seed ROI for DTI based tractography and to provide a more comprehensive, functionally related, white matter mapping, a very important tool used in pre-surgical mapping.

Introduction

The white matter possesses about 50% of the adult brain volume (Filley, 2001) and consists of a complex array of neuronal fiber networks. This network can be divided into specific tracts built of thousands of aligned neuronal fibers (axons) connecting different brain regions and target cells. Within the tracts, each fiber is usually coated with a multiple cell membrane layers (myelin) providing efficient and fast electrical transmission. Many brain diseases affect the white matter fibers either by disruption, degeneration or deviation of the fibers. Disruption of fiber continuity or disintegration of the myelin membrane surrounding the axons (demyelination) as what happens in multiple sclerosis is the most common form of white matter pathology. One of the less studied pathologies of white matter is displacement of neuronal fibers. Pressure applied on the white matter may lead to significant loss of neuronal transmission, demyelination and axonal loss leading to disability (Bergstrom et al., 1986; O'Brien et al., 1987; Siegal et al., 1987). Indeed, permanent damage to white matter integrity is known to occur in cases of severe and chronic exposure to mechanical intra-cranial pressure as happens in hydrocephalus (Del Bigio et al., 2003; Ding et al., 2001; Hanlo et al., 1997).

Diffusion tensor imaging (DTI) is an MRI based methodology that maps white matter (Basser and Pierpaoli, 1998; Pajevic and Pierpaoli, 1999; Pierpaoli and Basser, 1996; Pierpaoli et al., 1996) which has recently become extensively used for clinical purposes. DTI is based on the anisotropic nature of water motion in white matter fibers (Basser and Pierpaoli, 1998; Pierpaoli and Basser, 1996; Pierpaoli et al., 1996). Along the fibers, the motion of water molecules is relatively free, while perpendicular to them, it is more hindered. Based on this observation, DTI enables to extract the orientation of the fibers on a pixel by pixel basis and to quantify the motional anisotropy, with measures such as fractional anisotropy (FA) (Basser and Pierpaoli, 1998). FA was used over the last decade to study several white matter related diseases (Wieshmann et al., 1999; Tievsky et al., 1999; Pierpaoli et al., 2001; Takahashi et al., 2002; Sotak, 2002; Lim and Helpern, 2002; Horsfield and Jones, 2002; Holodny and

* Corresponding author. Department of Neurobiochemistry, Faculty of Life Sciences, Tel Aviv University, Tel Aviv 69978, Israel. Fax: +972 3 6973080.
E-mail address: assafyan@post.tau.ac.il (Y. Assaf).
Available online on ScienceDirect (www.sciencedirect.com).

1053-8119/$ - see front matter © 2005 Elsevier Inc. All rights reserved.
doi:10.1016/j.neuroimage.2005.11.015

Ollenschlager, 2002; Mori et al., 2002; Sinha et al., 2002; Witwer et al., 2002). Typically, disruption to organization of the fibers whether in the form of demyelination, axonal loss or other processes of cellular degeneration will cause a decrease of FA in white matter. One of the applications of DTI is to distinguish between distinct effects of SOLs (space occupying lesions) on white matter such as displacement of the tracts, destruction of the fibers or infiltration of the white matter tracts (Witwer et al., 2002; Mori et al., 1999). In contrast to the large number of studies on DTI in brain diseases, there are only a handful of reports on the investigation of white matter deviation by this technique. Barker's group (Eriksson et al., 2001; Wieshmann et al., 2000) was the first to show that DTI can help in delineation of displaced white matter fibers and suggested that the increased anisotropy might be related to white matter compression. Another work of mapping displaced white matter was done by Witwer et al. (2002), who used directionally color-coded maps (also termed: directionally encoded color (DEC)) mapping of DTI to mark displaced white matter as opposed to destructed or infiltrated white matter. Recently, Assaf et al. (2003) have shown that DTI measures could help in characterizing displaced white matter in 2D DEC-FA maps.

The introduction of 3D fiber tracking based on DTI extended the clinical use of this method for pre-surgical mapping (Mori et al., 1999, 2002). Fiber tractography enables three-dimensional visualization of specific fiber bundles that are either in proximity to a lesion or that are influenced by it. DTI based fiber tractography necessitates definition of a seed region of interest (ROI) that is located at the path of the investigated fiber network system in order to initiate the fiber tracking procedure (Basser et al., 2000; Conturo et al., 1997; Ito et al., 2002; Mori et al., 1999). Selecting seed ROIs based on known anatomical landmarks has led to the identification of a large number of fiber bundle systems in healthy subjects (Catani et al., 2002; Wakana et al., 2004). Fiber tractography was also used to investigate large white matter bundles in vicinity to brain lesions, particularly the pyramidal tract of the motor system (Akai et al., 2005; Berman et al., 2004; Clark et al., 2003; Hendler et al., 2003; Yamada et al., 2003; Stieltjes et al., 2001). However, brain lesions, especially SOLs, often affect the white matter and may alter the known anatomical path in which the fibers pass. Nonetheless, in many of these cases, only partial or no functional deficits are observed leading to the assumption that the fibers, though deviated, are still partially functionally intact. In such cases, white matter mapping using seed ROI based on known normal anatomical locations might be misleading, since the white matter is deviated from its normal location. This becomes even more complicated when edema masks the path of the white matter tracts. Recently, it has been shown that DTI based tractography can be combined with functional magnetic resonance imaging (fMRI) to mark both gray and white matter integrity and functionality in relation to brain lesions (Hendler et al., 2003; Parmar et al., 2004). In this work, we used fMRI driven seed ROI selection procedure in patients with SOLs where probable deviation of white matter tracts was observed.

Guye et al. (2003) have also proposed an approach where fMRI might help in defining a seed region of interest for functional connectivity mapping. While they showed that fMRI might help in identifying the seed ROI in the presence of SOL, they did not explore tracking or connectivity measures of different white matter pathologies in the presence of SOL. In this work, we specifically distinguish between cases of lesion infiltration into white matter and white matter displacement by a lesion. While tracking procedure might be successful in cases of displaced white matter, given the appropriate seed ROI, in infiltrated white matter, reduced fractional anisotropy might significantly complicate the tracking ability. Our aim is to show that the combination and co-registration of routinely used, clinically feasible, fMRI and DTI data to the same anatomical volume constrains the seed ROI selection procedure for fiber tracking. This procedure helps the tractographer to define seed ROI which are relevant to desired fiber system. The fMRI activated areas constrain the ROI selection to regions where desired, functionally related, fiber bundle pass. By using the fMRI activations as landmarks for the seed ROI selection, we were able to track the complete path of the fiber system when the fibers were displaced. Following the identification of the functional fiber system, we could then specifically characterize the effect of the SOL on the white matter. To that end, we used analysis of the principal diffusivities to characterize the displaced white matter.

Methods

Patients

Nine patients and five healthy subjects participated in this research. All the patients were referred to the fMRI clinic for pre-surgical functional mapping. The mapping included both regular anatomical MRI, functional MRI, which was designed to detect brain activity relevant to their lesion, and DTI based fiber tractography, in order to determine the involvement of white matter structures either in the lesioned area, or in the vicinity of the lesion. The DTI was used to estimate the displacement and edema/tumor infiltration to the white matter. In this manuscript, we focus on subjects where displacement of white matter occurs without noticeable edema or tumor infiltration to the displaced path of the fibers. Six of the patients in this research had lesions related to language skills: peri-inferior frontal gyrus (IFG, Broca's area), or peri-superior temporal sulcus (STS, Wernicke's area). Three patients had lesions related to motor activities in the pre-central gyrus area or along the pyramidal tract.

fMRI tasks

The fMRI experiment probing motor activity was a finger-tapping task, expected to show motor related activations in the pre-central gyrus (primary motor area) as well as activations related to planning of motor movements in the supplementary motor area (e.g., Tomczak et al., 2000). The language task used to probe activity in language related areas was a verb generation task which activates mainly the IFG and STS (e.g., Roux et al., 2003).

The motor finger-tapping paradigm consisted of a visually presented block design task with 44 volumes (including the first 6 volumes which were later discarded in analysis, to allow magnetization stabilization). Each volume acquisition was 3 s (see MRI parameters below). The design included 4 alternating blocks of task and rest (15 s for stimulus presented at rate of 0.5 Hz and 12 s for rest). During the task, the subjects moved their fingers according to numbers shown on a screen, slides with numbers changed every 2 s). During the rest period, subjects did not perform any action. The overall duration of the finger-tapping task was 2 min and 12 s. The Language task included 68 volumes (again first 6 volumes were discarded from the analysis). The design included

4 blocks of auditorily presented verb generation task interleaved with silence periods (4 stimulus blocks of 21 s and 4 silence blocks ranging from 18 to 27 s). During the task, subjects heard nouns through earphones and were asked to silently generate verbs related to the nouns presented. The overall duration of the language task was 3 min and 24 s.

MRI Parameters

fMRI

Experiments were performed on a 1.5 T Signa GE scanner. Functional MRI was scanned using gradient-echo echo-planar-imaging (GE-EPI) pulse sequence with the following parameters: TR/TE = 3000/55 ms, flip angle = 90°, 21 slices with thickness of 4 mm, 1 mm gap between slices, 80 × 80 matrix (reconstructed to 128 × 128) with an FOV of 24 × 24 cm^2.

DTI

Diffusion weighted images (DWIs) were acquired using a pulsed-gradient-spin-echo echo-planar-imaging (PGSE-EPI) with the following parameters: TR/TE = 10,000/98 ms, 48 slices with thickness of 3 mm, no gap between slices, 128 × 128 matrix with an FOV of 24 × 24 cm^2. The DWIs were acquired along 6 non-collinear gradient directions with b value of 1000 s/mm^2 (Δ/δ of 31/25 ms) according to Basser and Pierpaoli (1998), with an additional b = 0 image. The above protocol was repeated 3 times for signal averaging. Overall DTI acquisition time was approximately 5 min.

High-resolution anatomical MRI: for each subject a high-resolution anatomical data set was scanned. Scans included 3D spoiled gradient recalled echo (SPGR) sequence with the following parameters: TR/TE = 40/9 ms, flip angle = 30°, matrix of 256 × 256, FOV of 24 × 24 cm^2, ~70 axial slices of 2 mm thickness, no gap between slices. In cases where a contrast enhancement was needed, GdDTPA (0.5 mmol/kg) was injected prior to the SPGR acquisition. In addition T_2-weighted images were acquired with geometrical parameters identical to the DTI, using a fast spin-echo (FSE) sequence with the following parameters: TR/TE = 3000/102 ms, echo train length of 16 echoes and a matrix of 256 × 256. For one of the subjects, T_2-FLAIR images were sampled with the following parameters: TR/TE = 8000/140, TI = 2100, matrix of 256 × 256 and with the same geometrical parameters as the DTI.

Data analysis

The analysis for each technique (fMRI and DTI) was performed separately. The analysis was performed at the single subject data level, due to variability in the clinical cases and the nature and locations of their brain lesions.

fMRI analysis

Functional MRI analysis was performed using the BrainVoyager© software (version 4.9; Brain Innovation B.V., Maastricht, The Netherlands). Images were pre-processed to remove head motion artifacts and linear signal drifts. A voxel by voxel statistical analysis (Statistical analysis included hypothesis testing for significant correlation between the paradigms and the BOLD time course) of the contrast between the task and rest periods was performed and produced individual parametric maps for each task, with significantly activated voxels ($P < 0.001$, uncorrected) in the relevant ROIs. The whole brain volume with the activations was converted to Analyze file format using ImageJ (Rasband, 1997–2005).

DTI analysis

DTI scans were first re-aligned using SPM2 (2003, FIL, UCL, London, UK) (Friston et al., 1995) for motion correction and then analyzed using an in-house software in Matlab© (Mathworks, USA) according to a procedure given by Basser and Pierpaoli (1998).

The essence of this project was to mark the seed ROIs for fiber tracking on the directionality encoded color FA maps using the fMRI activations as seed points, rather than using the known anatomical locations (identified by using a DTI based white matter atlas, Wakana et al., 2004). For this purpose, we followed several steps: first, we performed co-registration and re-slicing of the high-resolution anatomical data (either SPGR, T_2 or FLAIR) of each subject to a single-subject anatomical template (same for all subjects) with the same geometrical parameters as the DTI scans (48 slices, 3 mm slice thickness, no gap, matrix of 128 × 128). Similar registration results were obtained for all high resolution anatomical data sets, and the one which demonstrated best the tumor was selected for each patient. The co-registration was done using SPM2 by a rigid body 12-mode linear transformation using the mutual information cost–function and trilinear algorithm for re-slicing with no wrapping or image masking. The down-sampling of the high-resolution data was done in order to provide similar resolution of the anatomical data set to that of the DTI and fMRI. Moreover, this ensured that both fMRI and DTI are co-registered while not artificially smoothed to a much higher resolution. In addition, using this procedure of co-registration and re-slicing to a template, we could later compare similar brain locations in all subjects. The next step was to co-register and re-slice the fMRI and DTI data to the down sampled anatomical data set co-registered to the template. The fMRI was co-registered using the first volume of the EPI scan as the source data set and the brain volume with the fMRI activations being co-registered and re-sliced in the same manner. As the DTI images contain directional information, the co-registration transformation matrix was also used to recalculate the b-matrix for each volume and each gradient direction to avoid artifactual tensor orientation calculation (Alexander et al., 2001).

Following the process described above, both the fMRI activations and the DTI data were co-registered and resliced according to the same anatomical data set. This enabled us to perform seed ROI selection driven by the locations of the co-registered fMRI activations. Seed ROIs were selected manually on the directionally encoded color FA maps (extracted from DTI using RGB encoding for the eigenvectors) adjacent to the relevant fMRI activation as a free form polygon. The whole fMRI activated area obtained by using a specific statistical threshold was regarded as a single cluster without referring to specific peak activations. The seed ROI for tractography was selected from a sphere of 15 voxels around the fMRI cluster, depending on the direction of the fibers approaching the fMRI activation for each fiber system: (A) for the pyramidal tract, the ROI was typically selected below the area of activation. (B) For the SLF, the ROI for Broca's area was selected superiorly to the activation, and for Wernicke's area, it was selected medially to the activation (see Fig. 3D). Size, shape and specific location of the ROI varied according to the architecture of the white matter surrounding the fMRI activations. ROI sizes ranged

from 25 to 50 voxels. Once seed ROIs were selected, fiber tractography was done using a modification of the FACT method (Mori et al., 1999). Here, we initiated 8 equally spaced fibers within each voxel with step size of 0.3 voxel length. Tracking was terminated when anisotropy level was below 0.25 or when fibers showed a steep turn (more than 65°). Following fMRI based tractography and identification of the displaced white matter, further analysis was performed on the identified displaced fiber locations along the tract, to determine the parallel (largest eigenvalue) and radial (smallest eigenvalue) diffusivities as measured by DTI. This was achieved by specifying ROIs along the displaced tract using the tractography fiber locations (Xue et al., 1999; Wilson et al., 2003; Glenn et al., 2003; Jones et al., 2003). The ROI was chosen based on pixels in which the fiber pass both for the healthy hemisphere (where seed ROI was selected anatomically) and for the diseased hemisphere (where seed ROI was selected using fMRI).

Results

In this work, we focused on the pyramidal tract (part of the corona radiata) and the superior longitudinal fasciculus (SLF, arcuate fasciculus), two large bundles of white matter that connect critical areas of motor and language function, respectively. Fig. 1 shows tracking of the pyramidal tract based on known anatomical landmarks for 3 healthy subjects. The anatomically based ROIs are all marked on the directionally encoded color FA maps (internal capsule) and FA maps (pre-central gyrus) of all three subjects (see yellow ROIs on enlarged maps in Fig. 1). As all brains were co-registered and re-sliced to the same brain template, the pyramidal tract anatomical seed ROIs were located in the same slices for all subjects (slice 29 and slice 42 out of 48 slices for the internal capsule and below the pre-central gyrus, respectively). The fiber tracking maps show distinct similarity between all subjects, thus implying minor inter-subjects variability for this fiber system. Fig. 2 shows the tracking of the SLF by selecting a seed ROI on the large white matter bundle that passes in an anterior–posterior direction (green area on the DEC-FA maps, second column in Fig. 2) above the lateral fissure. The SLF was located in slice 34 (out of 48 slices). The seed ROI was similarly placed for all subjects (see yellow rectangles in the middle column of Fig. 2). The computed fiber tracts shown in Fig. 2 resemble known histological and morphological mapping of the SLF, but in contrast to the pyramidal tract, the inter-subject variability seems to be greater.

Fig. 3 shows the comparison of anatomical and fMRI based seed ROI selection procedures for the tractography of the SLF for a healthy subject. This figure shows that both anatomical and functionally based landmarks provide similar tracking results (Figs. 3C and D, respectively). However, the fMRI landmarks constrain the tracking procedure to connect the IFG with the STS. The fact that we select the ROI near areas of activations ensures that the fiber will pass through these regions. On the other hand, using the anatomical landmark approach, there is a real possibility that the fibers will not reach the IFG due to inherent DTI limitations (e.g., splitting and crossing fibers, low anisotropy at cortical areas) as in the presented case (Fig. 3C).

Fig. 4 shows an example of a patient (male, right handed, 23 years old) with an SOL in the left parietal hemisphere. The patient

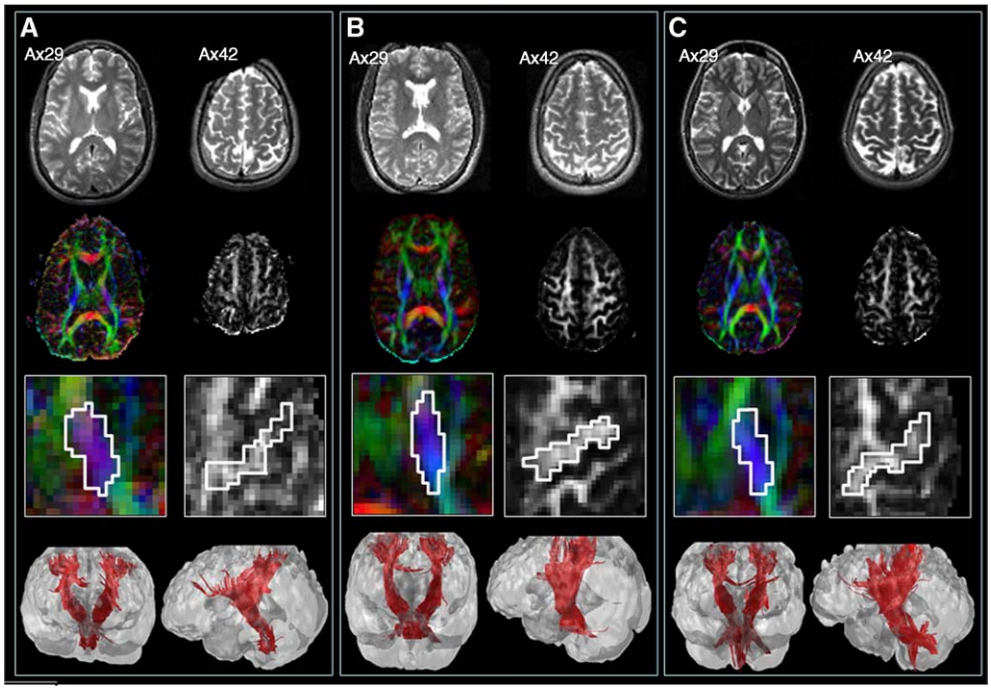

Fig. 1. Tracking of the motor system (pyramidal tract) based on anatomical landmarks. Panels A, B and C represent 3 healthy subjects. Top row shows T_2-weighted images of slices #29 and #42 out of 48 for each subject. Second row depicts the directionally encoded color maps (DEC) and fractional anisotropy (FA) maps (in gray scale) of the same slices. These slices were used to select seed ROIs for tracking. Third row shows enlargement of the brain slices shown above, and the line in white represents the seed ROI used for tracking. Left shows the fibers lying in the internal capsule, while on the right, the fibers shown lie below the post-central gyrus. The bottom row shows the computed fiber tracking maps based on the anatomical landmarks for front and side views of the brain.

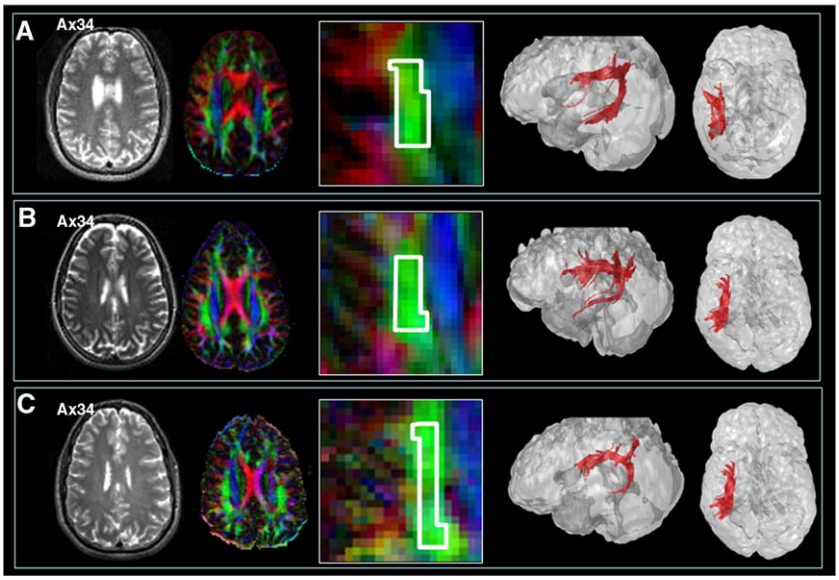

Fig. 2. Tracking of the superior longitudinal fascicles (SLF, arcuate fascicles) based on anatomical landmarks. Panels A, B and C represent 3 healthy subjects. Left column shows T_2-weighted images of slices #34 of 48 where the SLF typically passes. Second column shows the directionally encoded color FA maps of the same slice where the SLF is observed lateral to the ventricles and the corona radiata and shown in green (fibers crossing in an anterior–posterior direction). Middle column shows enlargement of the color coded FA maps upon which the seed ROI is marked in white. The two right columns show the computed fiber tracking maps for each of the subject from left-side and top brain views.

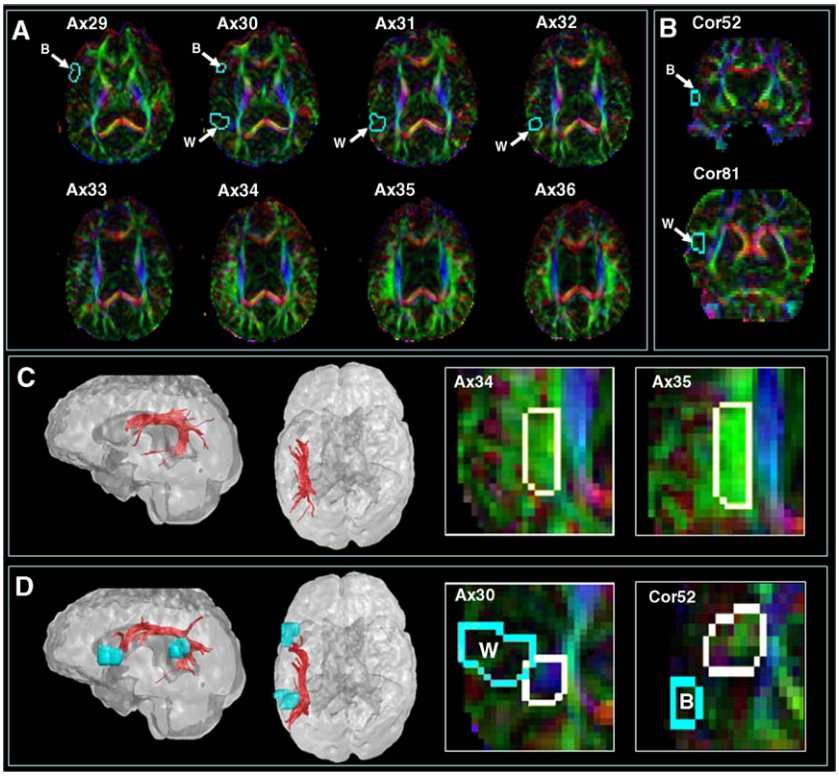

Fig. 3. Comparison of anatomically based and functionally based seed ROI selection procedures for the tractography of the SLF for a healthy subject. Panel A shows a sequence of DEC-FA axial slices (#29–36 of 48) with a cyan outline of the fMRI activated areas during a verb generation task (B represent Broca's area while W represents Wernicke's area). Panel B shows two DEC-FA coronal slices (#52 and #81) where the fibers leading to Broca's area and Wernicke's area can be seen. Panel C shows fiber tracking results based on anatomical landmarks (depicted on enlarged DEC-FA maps on the right, similar to Fig. 2). Panel D shows fiber tracking results based on fMRI landmarks (depicted on enlarged DEC-FA map on the right) both from left side and top brain views. Notice that both anatomically based and functionally based landmarks provide similar results. The tracking based on fMRI landmarks seem to be more complete as the SLF fibers reach the inferior frontal gyrus (IFG, Broca's area) where as in the anatomical landmark the fibers approach the IFG but end prematurely.

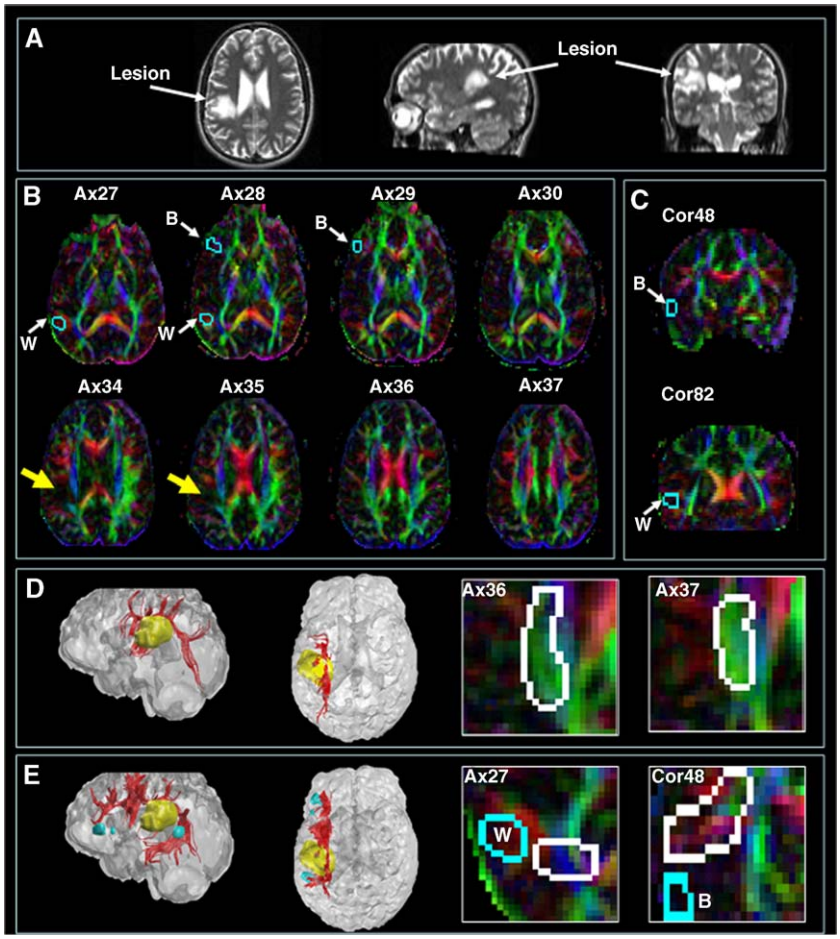

Fig. 4. A patient (male, 23 years old, right handed) with a space occupying lesion in the left parietal hemisphere located within the anatomical landmarks of the SLF. Panel A shows sagittal, coronal and axial T_2 slices with arrows indicating the location of the lesion. Panel B shows a series of axial DEC-FA maps at the level of the SLF with a cyan outline of the fMRI activated areas during a verb generation task (B represent Broca's area and W represents Wernicke's area). Panel C shows two DEC-FA coronal slices (#48 and #82) where the fibers leading to Broca's area and Wernicke's area can be seen. The appearance of fibers within the lesion seems to be poor and does not resemble their appearance in the contra lateral hemisphere (see yellow arrows on axial slices #34 and #35 that points to the lesion). Panel D shows fiber tracking results based on anatomical landmarks (depicted in white on enlarged DEC-FA maps on the right). The anatomical landmarks were chosen slightly above the typical location identified in healthy subjects (Fig. 2), suggesting that the fibers were displaced superiorly. Note that anatomical landmarks could not connect any of the functional areas found by fMRI. Panel E shows fiber tracking results based on fMRI landmarks (light blue areas on the 3D volume, ROI is depicted in white on enlarged DEC-FA map on the right) both from left side and top brain views. With this procedure, the SLF seems to be more complete revealing a significant displacement of the fibers superiorly above the lesion. This displacement could not be resolved using anatomical selection of the seed ROI.

presented with simple partial seizures. fMRI mapping of language related areas, IFG and STS, was concluded as within normal limits. The lesion was located within the typical anatomical landmarks of the SLF, however, the appearance of the fibers seemed poor compared to the contralateral side, indicating that the fibers might be either displaced or masked by massive lesion infiltration. The sagittal view (not shown) suggested that the fibers were displaced superiorly, thus the anatomical landmarks for this patient were chosen slightly above the typical location. Fiber tracking based on the modified anatomical landmarks (axial slices 36–37) resulted only in partial reconstruction of the fibers (Fig. 4D). Applying the fMRI based seed ROI approach (light blue volumes in Fig. 4E), a full reconstruction of the SLF was obtained, demonstrating the SLF displacement superiorly.

Fig. 5 shows an example of a patient (male, left handed, 26 years old) with a lesion in the anterior part of the left SLF. The patient suffered from simple partial seizures characterized by brief periods of aphasia. As in the previous case, the appearance of anisotropy within the lesion was low and significantly reduced compared with the contralateral hemisphere (Fig. 5B, axial slices 34–35). Axial (Fig. 5B), coronal (Fig. 5C) and sagittal (not shown) views did not provide any information regarding a possible deviation of the fibers, yet this possibility could not be excluded. Using anatomical landmarks, only a partial path of the SLF could be reconstructed (Fig. 5D) similar to the previous case (Fig. 4). Applying the fMRI based seed ROI approach based on the fMRI activation in Broca's and Wernicke's areas increased the number of identified fibers, but yet could not enable complete mapping of the SLF (Fig. 5E). Only when the tracking termination anisotropy threshold value was reduced to 0.1 (within the lesion), the tracking was successful showing a possible passage of the fibers through the edema (not shown). This figure presents a case where the seed ROI selection based on fMRI provided more but yet insufficient display of the fibers. This implies that this methodology could not compensate for some inherent DTI limitations (e.g., low FA values within edema).

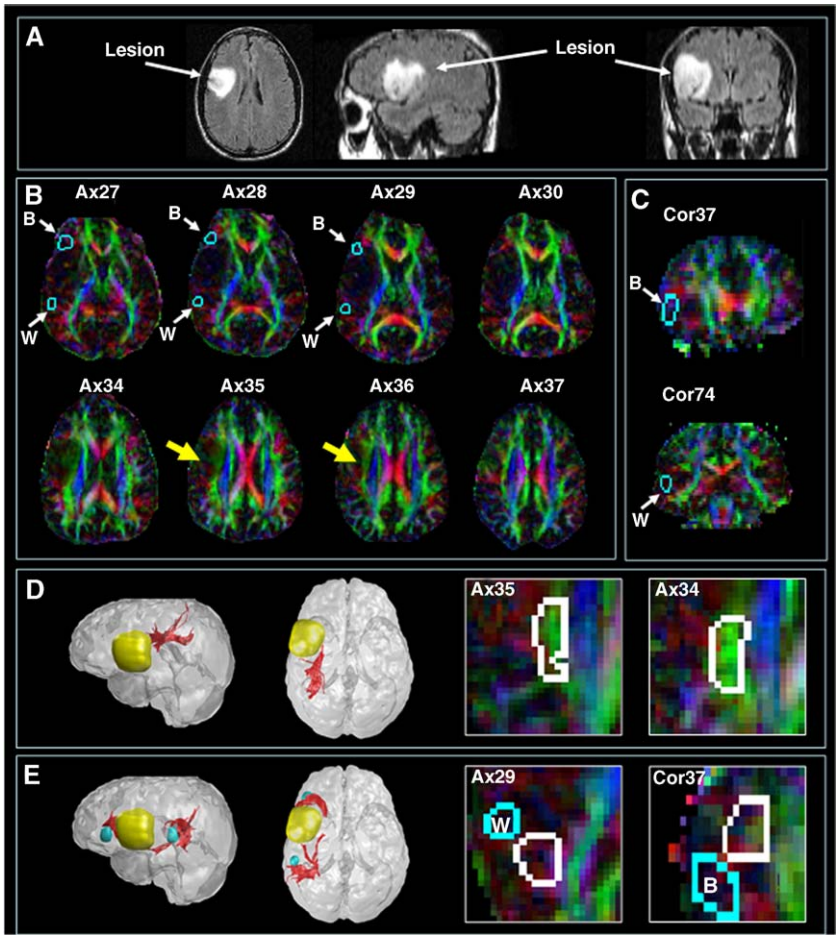

Fig. 5. A patient (male, 26 years old, left handed) with a space occupying lesion in the left parietal hemisphere located within the anatomical landmarks of the SLF. Panel A shows sagittal, coronal and axial FLAIR images with arrows indicating the location of the lesion. Panel B shows a series of axial DEC-FA maps at the level of the SLF with a cyan outline of the fMRI activated areas during a verb generation task (B represent Broca's area and W represents Wernicke's area). Yellow arrows indicate the location of the lesion. Panel C shows two DEC-FA coronal slices (#37 and #74) where the fibers leading to Broca's area and Wernicke's area can be seen. Appearance of fibers within the lesion seems to be masked by the massive edema (see yellow arrows on axial slices #35 and #36). Panel D shows fiber tracking results based on anatomical landmarks (depicted in white on enlarged DEC-FA maps on the right). The anatomical landmarks were chosen at similar anatomical location that was identified for the healthy subjects (Fig. 2). Note that anatomical landmarks could not connect any of the functional areas found by fMRI. Panel E shows fiber tracking results based on fMRI landmarks (light blue areas on the 3D volume, ROIs are depicted in white on enlarged DEC-FA map on the right) both from left side and top brain views. Even with this procedure, the SLF could not be tracked, and the fibers cannot be mapped when they reach the edema region. Probably, these fibers could be obtained if tracking FA threshold would have been lowered.

Fig. 6 presents an example of a patient (male, 26 years old) with a left frontal SOL extending to the area of the central sulcus. The patient suffered from episodes of right hand and leg weakness. Functional mapping of motor related activity revealed that the lesion displaced the hand primary motor areas laterally. The DEC-FA maps indicated that the lesion displaced the fibers inferiorly and posteriorly (Figs. 6B and C). Anatomically based ROI selection resulted in diffused tracking of fibers around the lesion. This approach does not enable selective differentiation between the motor related fibers (Fig. 6D). fMRI based ROI selection approach as shown in Fig. 6E enabled selective mapping of the hand related fibers. This approach provides additional, valuable pre-surgical information for the surgeon.

Once the displaced white matter fibers were identified, we performed a detailed analysis of the diffusion characteristics of the white matter in the vicinity of SOLs. Fig. 7 depicts an example for such analysis for a patient (male, right handed, 26 years old) with a fronto-temporal SOL which seemed to displace Broca's area anteriorly. Functional MRI based fiber tracking indicated a significant displacement of the SLF fibers (Fig. 7B). As the displaced fibers could now be identified, we selected a region of interest for quantitative analysis that included the pixels where the fibers pass (Fig. 7C). This was done using fMRI landmarks for the lesioned hemisphere and anatomical landmarks in the contra lateral hemisphere for comparison. Analysis of the ROIs used for quantitative analysis revealed an increase in FA (from 0.51 ± 0.04 to 0.58 ± 0.05), a decrease in the radial diffusivity (from $0.33 \pm 0.03 \times 10^{-5}$ cm^2/s to $0.27 \pm 0.06 \times 10^{-5}$ cm^2/s) and an increase in the parallel diffusivity (from $1.10 \pm 0.05 \times 10^{-5}$ cm^2/s to $1.21 \pm 0.05 \times 10^{-5}$ cm^2/s). We repeated this analysis for all patients (data summarized in Fig. 8). The first and main observation was that fractional anisotropy increased when white matter fibers were significantly displaced (Fig. 8A). FA increased from 0.43 ± 0.05 to 0.63 ± 0.06, showing an average increase of more than 40% for all patients. When analyzing the diffusivities (and not their summation index (FA)), we found a

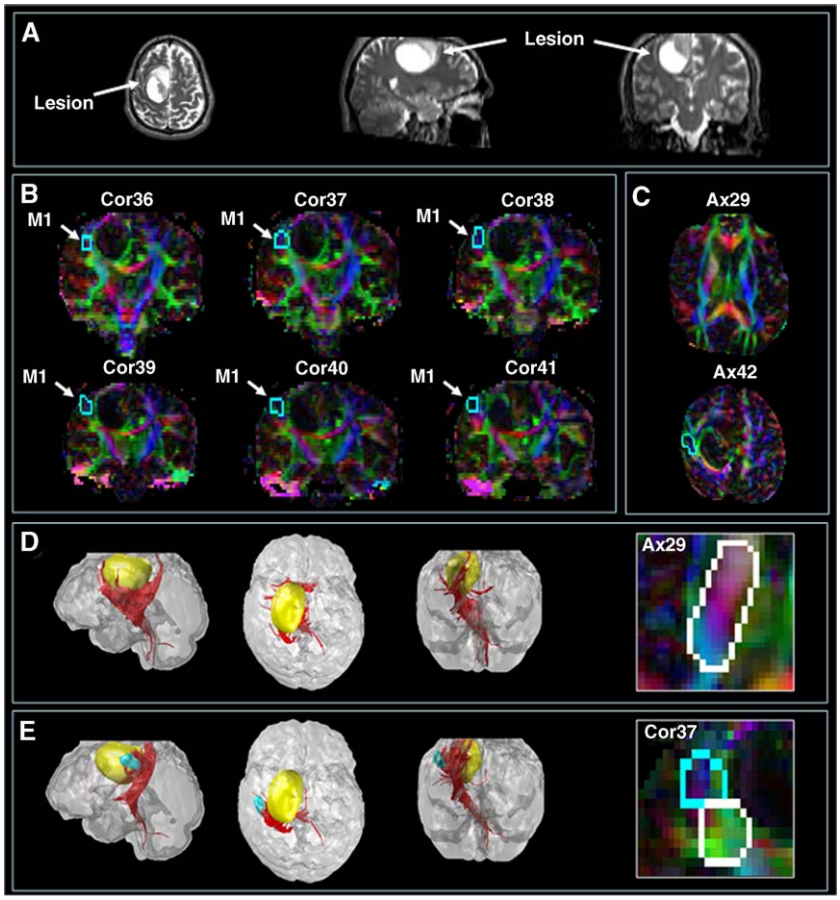

Fig. 6. A patient (male, 26 years old) with a left frontal SOL extending to the area of the central sulcus. Panel A shows sagittal, coronal and axial T_2 images with arrows indicating the location of the lesion. Panel B shows a series of coronal DEC-FA maps at the level of the pyramidal tract with a cyan outline of the fMRI activated areas during a finger tapping task (M1 represents the primary motor area corresponding with hand activation). Those images imply that the fibers are displaced both inferiorly and posteriorly by the lesion. Panel C shows two axial DEC-FA slices (#29 and #42) upon which anatomical landmarks are usually selected. Panel D shows fiber tracking results based on anatomical landmarks (depicted in white on enlarged DEC-FA map the right). The anatomical landmarks were chosen at similar anatomical locations that were identified for the healthy subjects (Fig. 1). Note that anatomical landmarks based fiber tracking detected a large number of fibers engulfing the lesion. Panel E shows fiber tracking results based on fMRI landmarks (light blue area on the 3D volume, ROI is depicted in white on enlarged DEC-FA map on the right) both from left side, top and rear brain views. This approach enables specific tracking of the fibers leading to the hand activated area.

decrease in the radial diffusivity (Fig. 8B) in contrast to an increase in the parallel diffusivity, similar to the single patient data presented in Fig. 7. The radial diffusivity (Fig. 8C) decreased from a value of $0.40 \pm 0.02 \times 10^{-5}$ cm^2/s in the healthy hemisphere to a value of $0.21 \pm 0.08 \times 10^{-5}$ cm^2/s around the SOL, a decrease of about 50%. In the same areas, the parallel diffusivity had slightly increased from $1.0 \pm 0.1 \times 10^{-5}$ cm^2/s in the healthy side to $1.2 \pm 0.2 \times 10^{-5}$ cm^2/s in the lesioned side, an increase of around 15%. Consequently, the mean ADC, which averages both the contribution of the parallel and radial diffusivities, remained unchanged (0.67 ± 0.05 vs. $0.69 \pm 0.06 \times 10^{-5}$ cm^2/s). These results are in line with our previous study on displaced white matter using DEC-FA (Assaf et al., 2003).

Discussion

This work indicated that incorporation of fMRI information could enhance the ability to identify tracts of interest in brains with deformed anatomy. DTI based fiber tractography attracts the attention of radiologists, neurologists and neurosurgeons as a possible way to visualize white matter paths in the diseased brain. Yet, in some of these cases due to brain pathology such as SOLs, the white matter fibers are displaced, thus exposing the tractography result to artifacts caused by the common analysis procedure. This approach uses seed ROI selection, based on known anatomical landmarks, according to DTI white matter atlas. Finding the route of the displaced fibers by utilizing trial and error might be successful in some cases but, at the same time, is highly prone to subjective decisions made by the analyzer. This trial and error might also include tempering with FA thresholds, which might lead to erroneous fiber tracking. Here, we suggested an approach that facilitates fiber tracking in clinical cases, based on combination of fMRI and DTI data thus constraining the seed ROI selection procedure. By doing this, we were able to show that in cases where tracking done by trial and error ended in incomplete mapping of the fibers, fMRI based seed ROI selection pointed to the altered path of the complete fiber system (Fig. 4).

Anatomical selection of seed ROI is used in the majority of works that deal with tractography in vicinity of brain lesions (Akai et al., 2005; Berman et al., 2004; Clark et al., 2003; Glenn et al., 2003; Jones et al., 2003; Wilson et al., 2003; Yamada et al., 2003; Stieltjes

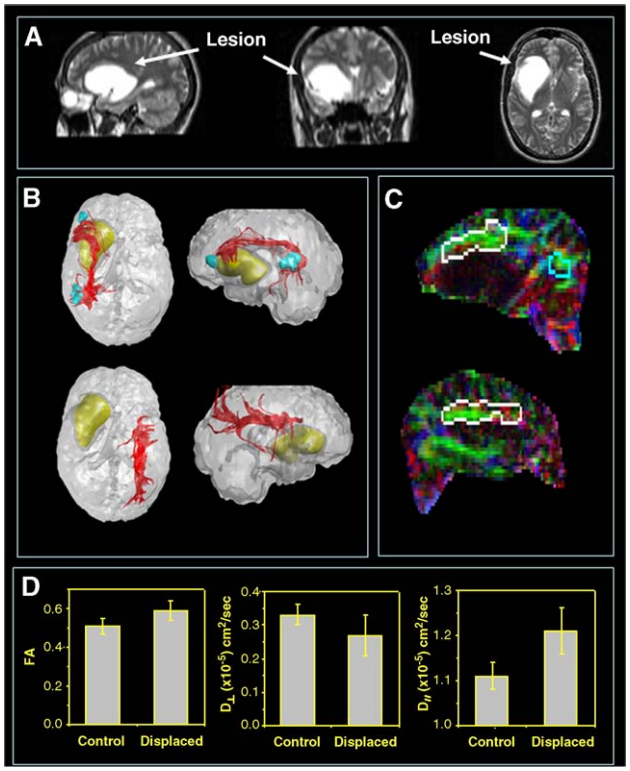

Fig. 7. A patient (male, 26 years old, right handed) with a left fronto-temporal space occupying lesion. Panel A shows sagittal, coronal and axial T_2 images with arrows indicating the location of the lesion. Panel B shows tracking of the SLF based on functional landmarks connecting Broca's and Wernicke's areas (light blue) with respect to the lesion (yellow) for the left hemisphere (top row). Bottom row of panel B shows tracking of the SLF for the right hemisphere based on anatomical landmarks. Panel C shows in white outline the pixels where the fibers pass on a sagittal DEC-FA map (one representative slice) for the left and right hemispheres. Panel D shows quantitative analysis of the FA, $D_{//}$ and $D_{\perp}$ for a region of interest selected along the reconstructed fibers of the lesion side and contra lateral side (control).

et al., 2001). Anatomically based ROI selection is considered a relatively reliable tractography method in healthy subjects (Fig. 1). Nevertheless, some white matter structures such as the SLF show higher variability in the tracking procedure, especially when approaching cortical areas (as shown in Fig. 2) (Makris et al., 2005). Tracking becomes even less reliable when an SOL distorts the anatomy on which the tracking is based (Figs. 4–6). In some cases, fibers lie adjacent to the lesion and are displaced by it (Fig. 4), whereas in other cases, fibers pass within the lesion (Fig. 5) or cannot be specifically identified (Fig. 6). Placement of the ROI based on anatomical landmarks in the vicinity of a lesion is subjective and may lead to miscalculation of the fibers path. In cases where displacement of the fibers occur, fMRI based seed ROI selection procedure may provide more reliable mapping of the fibers path.

The placement of anatomical seed ROI in healthy subjects is straightforward using a white matter atlas (Wakana et al., 2004; Catani et al., 2002). The tracking of the SLF is done by choosing a single ROI laterally to the corona radiata at the level of the higher edge of the ventricles (see Fig. 2). Placing additional ROIs at the mid-path of this bundle does not enhance the tractography. Only knowledge of the SLF end points (IFG and STS) might provide better results but those can be estimated accurately with fMRI (see Fig. 3). On the other hand, for the pyramidal tract, we use two ROIs (one at the level of the internal capsule and one below the central sulcus). The selection of two ROIs in this case significantly enhances the tracking result and provides a more complete appearance of the pyramidal tract. The need for two ROIs for complete tracking of the pyramidal tract arises due to the wide fanning of fibers into the cortex where one ROI is not sufficient to define the whole system. In cases of SOLs, we demonstrated that this procedure (anatomically based selection of ROI) may lead to artifactual results. To that end, we showed that by using fMRI landmarks for seed ROI selection we can enhance tracking performance. It is true that direct comparison between fMRI and anatomically based seed ROI selection in unfair mainly since in the one case we use a multiple ROI approach and in the other a single ROI. Indeed, the multiple ROI approach provided a more comprehensive reconstruction of the tracts. One might suspect that this is due to a larger number of seed voxels in the multiple ROI approach. Yet, we do not suggest that these two methods are comparable in any means. In patients with SOLs, anatomically based ROI selection (single or multiple) is wrong as the path of the fibers is unknown. Thus, we suggest here to identify a region or regions in which the desired fiber system passes using fMRI.

Recently, a similar approach (i.e., fMRI based seed ROI selection) has been used by Guye et al. (2003). There, the authors used an automatic placement of the seed ROI below the local maxima of the fMRI activations following a motor related task. They were able to show connectivity maps of the pyramidal tract

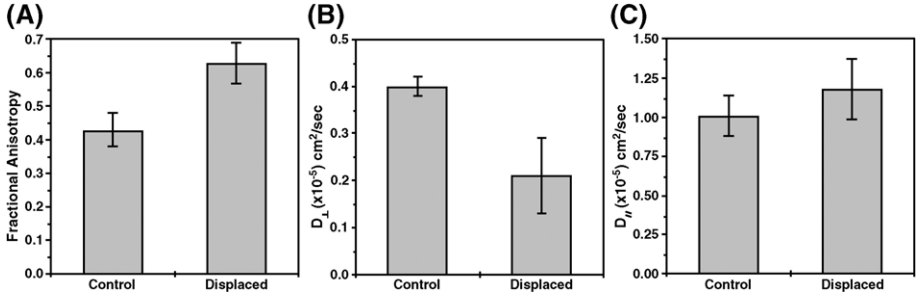

Fig. 8. Analysis of the diffusion properties of displaced and contralateral white matter tracts (averaged for 8 patients). Significant changes revealed in DTI measures of the displaced fiber tracts, compared to the opposite healthy hemisphere. (A) Fractional anisotropy increased when white matter fibers were significantly displaced, showing an average increase of more than 40%. The radial diffusivity decreased by about 50% in areas of displaced white matter (B), while the parallel diffusivity increased by more than 15% (C). The overall mean diffusivity (trace) did not change (data not shown). The ROIs for the quantitative analysis were selected using the tractography procedure. This procedure was done using the fMRI based approach (for displaced fibers) and anatomically based approach (for contralateral fibers).

based on DTI measures both in healthy and diseased subjects. We used a similar approach in a variety of patients with lesions affecting either the pyramidal tract or the SLF, infiltrating and/or displacing the fibers. From our experience, a distinction should be made between cases where the lesion infiltrates the white matter (tumor infiltration, edema) and cases where the fibers are displaced by the lesion mass. White matter infiltration of the lesion might lead to morphological changes in the tissue that will reduce the ability to reliably track the fibers. To that end, measurements of connectivity or anisotropy within a lesion are subject to the degree of edema or tissue deformation (Guye et al., 2003).

Even in cases of displaced white matter, where fMRI based ROI selection may provide reliable fiber tracking, the placement of the ROI should be done with care due to variability in fiber directions approaching the cortex, caused by the location of the SOL. This is more pronounced when tracking the SLF rather than the pyramidal tract, as this bundle is more directionally heterogeneous even in normal subjects (Figs. 2, 3). Thus, in this work, we placed the ROI manually surrounding the fMRI activation and detected the most reasonable ROI that should be selected. Under this approach, the area, location and size of the ROI varied from patient to patient. Indeed for a heterogenic and broad pathology such as space occupying lesions, an automatic definition of ROI would require a complicated algorithm. While Guye et al. (2003) placed the ROI below the local maxima of the motor fMRI activation in an automated manner; we placed it manually within a sphere of 15 voxels around the fMRI activation. Choosing the seed ROI below the fMRI activation might be successful for the pyramidal tract but insufficient for other fiber systems. Placing the ROI manually has the advantages of defining the specific fiber system we wish to track but has the disadvantage of being relatively subjective. One way to avoid subjective placement of the seed ROI is by using a "brute force" method constructing all of the fibers going through the 15 voxel sphere around the fMRI cluster. Using a "brute force" approach can also resolve the issue of the number of seed voxels used as raised above.

An additional advantage of using fMRI based ROI selection is the ability to selectively define distinct functionally related bundles. This is relevant to fiber systems that connect multiple functional areas (e.g., hand vs. leg motor functions). This is important in the clinical setting as it provides specific pre surgical information of the functional system (Fig. 6). Besides selectivity, the mutual constrains of fMRI and DTI based tracking ensure a more complete depiction of the fiber system (Fig. 3).

In order to characterize the pathophysiological condition of the displaced fibers, we evaluated the different diffusion measures along their path. In most white matter disorders and diseases, the fractional anisotropy is usually decreased compared to healthy tissue. Indeed, within the lesion, we also found reduced FA, as expected. By contrast, a significant increase in the FA was found in white matter tracts displaced by the lesion (Figs. 7, 8). These changes were not homogenous along the path of the fibers, and some areas within the selected ROI showed even higher FA values. Commonly, FA reduction in white matter diseases is characterized by an increase in the radial diffusivity, thus increasing the mean ADC. On the other hand, in the cases presented here, the radial diffusivity was reduced, while the parallel diffusivity was increased, leading to an overall increase in FA with no apparent change in the ADC. An increase in the density and tension of the fibers can be suggested as a possible mechanism for this observation (Assaf et al., 2003). An alternative explanation could be an increase in the homogeneity of the fiber system by a tighter alignment of the fibers within the fiber bundle. The ability to measure the diffusion characteristics of a specific fiber bundle provides quantitative means for estimation of pressure effects, both pre- and post-surgery as well as in follow up evaluation of the fiber's integrity. This could have an impact on patient management and also support other clinical and radiological observations.

DTI is a relatively new methodology and new insights regarding the analysis and interpretations of the results are published frequently. For instance, it is well known that DTI is unable to resolve white matter architecture in areas where more than one fiber population occupies the same voxel (Pierpaoli and Basser, 1996; Jones, 2003; Wiegell et al., 2000). In such areas, the diffusion anisotropy is artifactually reduced and reaches values similar to those of gray matter and CSF. In addition, eddy current induced image artifact, and physiological noise reduces the significance of the results and increases the standard deviation of the measurement (Horsfield, 1999). Solutions to these problems become more applicable in the form of multiple tensor field regularization (Tuch et al., 2002; Pasternak et al., 2005) and mutual information image registration procedures (Horsfield, 1999; Rohde et al., 2004). However, once overcoming the abovementioned problems, the two methodologies, DTI and fMRI, suffer from other inherent problems which make the registration between the two a complicated task. For instance, it is well known that better tracking can be done when more gradient orientations are acquired (Jones, 2004). However, high angular resolution of the gradient acquisition scheme may result in longer experimental times in which the analysis is prone to suffer more from significant patient head movements. Indeed, even at the very short experimental times, head movements may alter the correct estimation of fiber orientation. As for fMRI, in many cases, this method shows spread activation patterns, from which it is hard to point on the exact location of the functional region. In addition, both methodologies suffer from susceptibility induced geometrical image distortions, which necessitate advanced post-processing (Rohde et al., 2004). All of these problems lead to reduced reproducibility and reliability of each method alone.

Despite the problems mentioned above, careful analysis and the multi-method co-registration procedure presented in this paper can provide, in most cases, a reliable presentation of the functional network. Although each of the methodologies suffer from its own inherent artifacts, when combined, their constraints enhance the interpretation of the observations.

Acknowledgments

The authors wish to thank the following funds for financial support: The ministry of science and technology (The Eshkol program, to YA), The Israel Science Foundation (To YA), The Adams Super Center for Brain Research of Tel Aviv University (To TH and YA) and The Levie-Gitter-Edershiem institute for functional brain imaging (to TS). We also wish to thank the neurosurgeons and the patients who participated in this study.

References

Akai, H., Mori, H., Aoki, S., Masutani, Y., Kawahara, N., Shibahara, J., Ohtomo, K., 2005. Diffusion tensor tractography of gliomatosis cerebri. J. Comput. Assist. Tomogr. 29, 127–129.

Alexander, D.C., Pierpaoli, C., Basser, P.J., Gee, J.C., 2001. Spatial transformations of diffusion tensor magnetic resonance images. IEEE Trans. Med. Imaging 20, 1131–1139.

Assaf, Y., Pianka, P., Rothstein, P., Sigal, M., Hendler, T., 2003. Deviation of fiber tracts in the vicinity of brain lesions: evaluation by diffusion tensor imaging. Isr. J. Chem. 43, 155–163.

Basser, P.J., Pierpaoli, C., 1998. A simplified method to measure the diffusion tensor from seven MR images. Magn. Reson. Med. 39, 928–934.

Basser, P.J., Pajevic, S., Pierpaoli, C., Duda, J., Aldroubi, A., 2000. A. In vivo fiber tractography using DT-MRI data. Magn. Reson. Med. 44, 625–632.

Bergstrom, K., Thuomas, K.A., Ponten, U., Nilsson, P., Zwentnow, N.N., Vlajkovic, S., 1986. Magnetic resonance imaging of brain tissue displacement and brain water contents during progressive brain compression. An experimental study in dogs. Acta Radiol., Suppl. 369, 350–352.

Berman, J.I., Berger, M.S., Mukherjee, P., Henry, R.G., 2004. Diffusion tensor imaging guided tracking of fibers of the pyramidal tract combined with intraoperative cortical stimulation mapping in patients with gliomas. J. Neurosurg. 101, 66–72.

Catani, M., Howard, R.J., Pajevic, S., Jones, D.K., 2002. Virtual in vivo interactive dissection of white matter fasciculi in the human brain. NeuroImage 17, 77–94.

Clark, C.A., Barrick, T.R., Murphy, M.M., Bell, B.A., 2003. White matter tracking in patients with space-occupying lesions of the brain: a new technique for neurosurgical planning? NeuroImage 20, 1601–1608.

Conturo, T.E., Lori, N.F., Cull, T.S., Akbudak, E., Snyder, A.Z., Shimony, J.S., McKinstry, R.C., Burton, H., Raichle, M.E., 1997. Tracking neuronal fiber pathways in the living human brain. Proc. Natl. Acad. Sci. U. S. A. 96, 10422–10427.

Del Bigio, M.R., Wilson, M.J., Enno, T., 2003. Chronic hydrocephalus in rats and humans: white matter loss and behavior changes. Ann. Neurol. 53, 337–346.

Ding, Y., McAllister II, J.P., Yao, B., Yan, N., Canady, A.I., 2001. Axonal damage associated with enlargement of ventricles during hydrocephalus: a silver impregnation study. Neurol. Res. 23, 581–587.

Eriksson, S.H., Rugg-Gunn, F.J., Symms, M.R., Barker, G.J., Duncan, J.S., 2001. Diffusion tensor imaging in patients with epilepsy and malformations of cortical development. Brain 124, 617–626.

Filley, C.M. (Ed.), 2001. The Behavioral Neurology of White Matter. Oxford Univ. Press, New York, NY.

Friston, K.J., Ashburner, J., Frith, C., Poline, J.B., Heather, J.D., Frackowiak, R.S.J., 1995. Spatial registration and normalization of images. Hum. Brain Mapp. 2, 165–189.

Glenn, O.A., Henry, R.G., Berman, J.I., Chang, P.C., Miller, S.P., Vigneron, D.B., Barkovich, A.J., 2003. DTI-based three-dimensional tractography detects differences in the pyramidal tracts of infants and children with congenital hemiparesis. J Magn. Reson. Imaging 18, 641–648.

Guye, M., Parker, G.J., Symms, M., Boulby, P., Wheeler-Kingshott, C.A., Salek-Haddadi, A., Barker, G.J., Duncan, J.S., 2003. Combined functional MRI and tractography to demonstrate the connectivity of the human primary motor cortex in vivo. NeuroImage 19, 1349–1360.

Hanlo, P.W., Gooskens, R.J., van Schooneveld, M., Tulleken, C.A., van der Knaap, M.S., Faber, J.A., Willemse, J., 1997. The effect of intracranial pressure on myelination and the relationship with neurodevelopment in infantile hydrocephalus. Dev. Med. Child Neurol. 39, 286–291.

Hendler, T., Pianka, P., Sigal, M., Kafri, M., Ben-Bashat, D., Constantini, S., Graif, M., Fried, I., Assaf, Y., 2003. Delineating gray and white matter involvement in brain lesions: 3D alignment of fMRI and DTI. J. Neurosurg. 99, 1018–1027.

Holodny, A.I., Ollenschlager, M., 2002. Diffusion imaging in brain tumors. Neuroimaging Clin. N. Am. 12, 107–124.

Horsfield, M.A., 1999. Mapping eddy current induced fields for the correction of diffusion-weighted echo planar images. Magn. Reson. Imaging. 17 (9), 1335–1345.

Horsfield, M.A., Jones, D.K., 2002. Applications of diffusion-weighted and diffusion tensor MRI to white matter diseases—A review. NMR Biomed. 15, 570–577.

Ito, R., Mori, S., Melhem, E.R., 2002. Diffusion tensor brain imaging and tractography. Neuroimaging Clin. N. Am. 12, 1–19.

Jones, D.K., 2003. Determining and visualizing uncertainty in estimates of fiber orientation from diffusion tensor MRI. Magn. Reson. Med. 49, 7–12.

Jones, D.K., 2004. The effect of gradient sampling schemes on measures derived from diffusion tensor MRI: a Monte Carlo study. Magn. Reson. Med. 51, 807–815.

Jones, D.K., Catani, M., Reeves, S.J.C., Shergill, S.S., O'Sullivan, M., McGuire, P., Horsfield, M.A., Simmons, A., Williams, S.C., Howard, R.J., 2003. A tractography approach for studying fronto-temporal fasciculi in schizophrenia and schizophrenia like psychosis. Proc. Int. Soc. Magn. Reson. Med. 11, 244.

Lim, K.O., Helpern, J.A., 2002. Neuropsychiatric applications of DTI—A review. NMR Biomed. 15, 587–593.

Makris, N., Kennedy, D.N., McInerney, S., Sorensen, A.G., Wang, R., Caviness Jr., V.S., Pandya, D.N., 2005. Segmentation of subcomponents within the superior longitudinal fascicle in humans: a quantitative, in vivo, DT-MRI study. Cereb. Cortex 15, 854–869.

Mori, S., Crain, B.J., Chacko, V.P., van Zijl, P.C.M., 1999. Three-dimensional tracking of axonal projections in the brain by magnetic resonance imaging. Ann. Neurol. 45, 265–269.

Mori, S., Frederiksen, K., van Zijl, P.C., Stieltjes, B., Kraut, M.A., Solaiyappan, M., Pomper, M.G., 2002. Brain white matter anatomy of tumor patients evaluated with diffusion tensor imaging. Ann. Neurol. 51, 377–380.

O'Brien, J.P., Mackinnon, S.E., MacLean, A.R., Hudson, A.R., Dellon, A.L., Hunter, D.A., 1987. A model of chronic nerve compression in the rat. Ann. Plast. Surg. 19, 430–435.

Pajevic, S., Pierpaoli, C., 1999. Color schemes to represent the orientation of anisotropic tissues from diffusion tensor data: application to white matter fiber tract mapping in the human brain. Magn. Reson. Med. 42, 526–540.

Parmar, H., Sitoh, Y.Y., Yeo, T.T., 2004. Combined magnetic resonance tractography and functional magnetic resonance imaging in evaluation of brain tumors involving the motor system. J. Comput. Assist. Tomogr. 28, 551–556.

Pasternak, O., Sochen, N., Assaf, Y., 2005. Variational regularization of multiple diffusion tensor fields. In: Weickert, J., Hagen, H. (Eds.), Visualization and Processing of Tensor Fields. Springer, Berlin.

Pierpaoli, C., Basser, P.J., 1996. Towards a quantitative assessment of diffusion anisotropy. Magn. Reson. Med. 36, 893–906.

Pierpaoli, C., Jezzard, P., Basser, P.J., Barnett, A., Di Chiro, G., 1996. Diffusion tensor MR imaging of the human brain. Radiology 201, 637–648.

Pierpaoli, C., Barnett, A., Pajevic, S., Chen, R., Penix, L.R., Vitra, A., Basser, P., 2001. Water diffusion changes in Wallerian degeneration and their dependence on white matter architecture. NeuroImage 13, 1174–1185.

Rasband, W.S., 1997–2005. ImageJ, U. S. National Institutes of Health, Bethesda, Maryland, USA, http://rsb.info.nih.gov/ij/.

Rohde, G.K., Barnett, A.S., Basser, P.J., Marenco, S., Pierpaoli, C., 2004. Comprehensive approach for correction of motion and distortion in diffusion-weighted MRI. Magn. Reson. Med. 51 (1), 103–114.

Roux, F.E., Boulanouar, K., Lotterie, J.A., Mejdoubi, M., LeSage, J.P., Berry, I., 2003. Language functional magnetic resonance imaging in preoperative assessment of language areas: correlation with direct cortical stimulation. Neurosurgery 52 (6), 1335–1347.

Siegal, T., Siegal, T.Z., Sandbank, U., Shohami, E., Shapira, J., Gomori, J.M., Ben-David, E., Catane, R., 1987. Experimental neoplastic spinal cord compression: evoked potentials, edema, prostaglandins, and light and electron microscopy. Spine 12, 440–448.

Sinha, S., Bastin, M.E., Whittle, I.R., Wardlaw, J.M., 2002. Diffusion tensor MR imaging of high-grade cerebral gliomas. Am. J. Neuroradiol. 23, 520–527.

Sotak, C.H., 2002. The role of diffusion tensor imaging in the evaluation of ischemic brain injury—A review. NMR Biomed. 15, 561–569.

Stieltjes, B., Kaufmann, W.E., van Zijl, P.C., Fredericksen, K., Pearlson, G.D., Solaiyappan, M., Mori, S., 2001. Diffusion tensor imaging and axonal tracking in the human brainstem. NeuroImage 14 (3), 723–735.

Takahashi, S., Yonezawa, H., Takahashi, J., Kudo, M., Inoue, T., Tohgi, H., 2002. Selective reduction of diffusion anisotropy in white matter of Alzheimer disease brains measured by 3.0 Tesla Magnetic Resonance Imaging. Neurosci. Lett. 332, 45–48.

Tievsky, A.L., Ptak, T., Farkas, J., 1999. Investigation of apparent diffusion coefficient and diffusion tensor anisotropy in acute and chronic multiple sclerosis lesions. Am. J. Neuroradiol. 20, 1491–1499.

Tomczak, R.J., Wunderlich, A.P., Wang, Y., Braun, V., Antoniadis, G., Gorich, J., Richter, H.P., Brambs, H.J., 2000. fMRI for preoperative neurosurgical mapping of motor cortex and language in a clinical setting. J. Comput. Assist. Tomogr. 24 (6), 927–934.

Tuch, D.S., Reese, T.G., Wiegell, M.R., Makris, N., Belliveau, J.W., Wedeen, V.J., 2002. High angular resolution diffusion imaging reveals intravoxel white matter fiber heterogeneity. Magn. Reson. Med. 48, 577–582.

Wakana, S., Jiang, H., Nagae-Poetscher, L.M., Van-Zijl, P.C.M., Mori, S., 2004. Fiber track-based atlas of human white matter anatomy. Radiology 230, 77–87.

Wiegell, M.R., Larsson, H.B., Wedeen, V.J., 2000. Fiber crossing in human brain depicted with diffusion tensor MR imaging. Radiology 217, 897–903.

Wieshmann, U.C., Clark, C.A., Symms, M.R., Franconi, F., Barker, G.J., Shorvon, S.D., 1999. Reduced anisotropy of water diffusion in structural cerebral abnormalities demonstrated with diffusion tensor imaging. Magn. Reson. Imaging 17, 1269–1274.

Wieshmann, U.C., Symms, M.R., Parker, G.J., Clark, C.A., Lemieux, L., Barker, G.J., Shorvon, S.D., 2000. Diffusion tensor imaging demonstrates deviation of fibers in normal appearing white matter adjacent to a brain tumour. J. Neurol., Neurosurg. Psychiatry 68, 501–503.

Wilson, M., Tench, C.R., Morgan, P.S., Blumhardt, L.D., 2003. Pyramidal tract mapping by diffusion tensor magnetic resonance imaging in multiple sclerosis: improving correlations with disability. J. Neurol., Neurosurg. Psychiatry 74, 203–207.

Witwer, B.P., Moftakhar, R., Hasan, K.M., Deshmukh, P., Haughton, V., Field, A., Arfanakis, K., Noyes, J., Moritz, C.H., Meyerand, M.E., Rowley, H.A., Alexander, A.L., Badie, B., 2002. Diffusion tensor imaging of white matter tracts in patients with cerebral neoplasm. J. Neurosurg. 97, 568–575.

Yamada, K., Kizu, O., Mori, S., Ito, H., Nakamura, H., Yuen, S., Kubota, T., Tanaka, O., Akada, W., Sasajima, H., Mineura, K., Nishimura, T., 2003. Brain fiber tracking with clinically feasible diffusion tensor MR imaging: Initial experience. Radiology 227, 295–301.

Xue, R., van Zijl, P.C., Crain, B.J., Solaiyappan, M., Mori, S., 1999. In vivo three-dimensional reconstruction of rat brain axonal projections by diffusion tensor imaging. Magn. Reson. Med. 42, 1123–1127.